Role of the electronic state of cerium in the magnetic properties of $CeNi_xPt_{1-x}$ compounds

José Ignacio Espeso
Departamento de Física Moderna, Universidad de Cantabria, Avda. de los Castros s/n, 39005 Santander, Spain

José Carlos Gómez Sal
CITIMAC, Universidad de Cantabria, Avda. de los Castros s/n, 39005 Santander, Spain

Jesús Chaboy
Instituto de Ciencia de Materiales de Aragón and Departamento de Física de la Materia Condensada, CSIC-Universidad de Zaragoza, 50009 Zaragoza, Spain

(Received 29 February 2000; revised manuscript received 27 June 2000; published 12 December 2000)

We present in this work an x-ray absorption spectroscopy investigation performed at the $L_{1,3}$ edges of Ce in the intermetallic compounds $CeNi_xPt_{1-x}$. This study provides a direct microscopic probe of the cerium electronic state that is found to be trivalent up to $x \leqslant 0.9$ and an intermediate valence for higher Ni content. The modification of the Ce L_3- and L_1-edge absorption profiles has been correlated with the density of conduction electrons and with the modification of the hybridization between the orbitals of Ce and the conduction band. Our results stressed that the behavior of the $CeNi_xPt_{1-x}$ series is in agreement with the Doniach diagram only up to $x \leqslant 0.9$. Moreover, the transition to nonmagnetism is due to the progressive screening of the $4f$ shell as the result of the competition between exchange interactions and the Kondo effect and not to the change of cerium valence.

DOI: 10.1103/PhysRevB.63.014416 PACS number(s): 75.20.Hr, 75.30.Mb, 61.10.Ht

I. INTRODUCTION

The most unusual physical properties appearing in the cerium-based intermetallic compounds are classified as Kondo lattices,[1] heavy fermions,[2] or intermediate valence behavior.[3] The main characteristic in these compounds is the resulting strong $4f$ conduction-band hybridization, and the standard theoretical models determine the ground state as the result of the competition between the intrinsic Ruderman-Kittel-Kasuya-Yosida (RKKY) interaction and the onsite Kondo coupling. The characteristic energies for these two interactions are $T_{RKKY} \propto (|J_k \rho_c|)^2$ and $T_k \propto \exp(-1/|J_k \rho_c|)$. ρ_c is the density of states at the Fermi level and $J_k \propto |V_{cf}|^2/(E_F - E_f)$ is the exchange-coupling strength between $4f$ and conduction electrons, which depends on the c-f hybridization (V_{cf}) and the location of the $4f$ level (E_f) relative to the Fermi energy (E_F). When the RKKY interaction dominates ($T_{RKKY} > T_K$), the system orders magnetically. For a comparable strength of these two interactions ($T_{RKKY} \approx T_K$), the system shows Kondo-type behavior, but still orders magnetically. When Kondo-type interactions dominate ($T_K > T_{RKKY}$), the system is demagnetized due to the Kondo effect and the ground state is nonmagnetic. This competition is described by the well-known Doniach diagram,[4] in which the characteristic energies for these two interactions are plotted vs $|J_k \rho_c|$. Although the Doniach model provides a qualitative description of the main experimental features of Kondo lattices, detailed comparison to experiments is made difficult other than for small hybridization between local moments and conduction electrons.

Despite the fact this model is currently used,[5] several reports dealing with the coexistence of magnetic correlations and the Kondo effect have been recently published trying to re-examine the Doniach diagram.[6–8] Recent experimental results on the $CeRu_2Ge_2$ system[9] appear to be in qualitative agreement with a revisited Doniach model.[6,7] The early model[6] is restricted to the case of a half-filled conduction band that is of relevance for Kondo insulators. More recently, it has been improved by including the effect of conduction-band filling that is important for metallic and underscreened systems.[7] However, the treatment of both models cannot describe magnetically ordered states, and, consequently, does not address the competition between the Kondo effect and long range magnetic order.

When discussing their model, Iglesias, Lacroix, and Coqblin[6] consider that $CeSi_x$ and $CeNi_xPt_{1-x}$ are not relevant for their study since the experimentally observed transition to nonmagnetism corresponds to a change of the valence of the cerium atoms. However, it should be pointed out that the $CeNi_xPt_{1-x}$ series[10] is reported as one of the best examples of a ferromagnetic dense Kondo system in which the variations of both the Curie temperature, T_c, and the Kondo temperature, T_K, as functions of the Ni content, are similar to those predicted in the Kondo lattice model.[11]

CePt is a moderate Kondo ferromagnet ($T_c = 5.8$ K) with a magnetic moment slightly reduced with respect to the Ce^{3+} free ion value,[10] while CeNi behaves as a Pauli paramagnet.[12] CeNi is considered an example of an intermediate valence compound, and it has received great attention over the last years because of its anisotropic effects on thermal expansion and magnetostriction,[13,14] its anomalous lattice dynamics,[15] and its peculiar Fermi surface.[16] For intermediate Ni substitutions the $CeNi_xPt_{1-x}$ system exhibits the hallmarks of a system where $4f$ conduction-band hybridization increases with decreasing cell volume.[17] This has been confirmed by studying the modification of $|J_k \rho_c|$ due to the increase (decrease) of the cell volume in the diluted $Ce_yLa_{1-y}Ni_xPt_{1-x}$ ($Ce_yY_{1-y}Ni_xPt_{1-x}$) compounds.[18,19] For

the lowest Ce concentrations, a tendency to a Kondo impurity behavior was found.[19–21]

In the $CeNi_xPt_{1-x}$ system the long-range magnetic order disappears around $x=0.9$. Although the macroscopic behavior of this series (γ electronic coefficient, magnetic moment reduction, etc.) is well understood in the framework of a simple resonance model,[22] it is not clear how this evolution takes place at the microscopic scale. Then, the one open problem of this series is the interplay between the cerium electronic state and the magnetic properties driven by Ni substitution. Indeed, earlier works invoke that there is a continuous evolution from a Ce^{3+} magnetic state in CePt to an intermediate valence state in CeNi.[10] The proposed mechanism is that by substituting progressively Pt by Ni, the Fermi level draws nearer the $4f$ level, leading to an increase of $|J_k\rho_c|$. From the analysis of the cell parameters' behavior it was concluded that the intermediate valence state emerges for $x \geqslant 0.8$. These conclusions are in qualitative agreement with former Ce L_3-edge x-ray absorption spectroscopy (XAS) results, showing a continuous increase of the Ce valence from 3 in CePt to 3.11 for CeNi.[23]

However, from both magnetization measurements and neutron diffraction,[24] the observed behavior is a progressive reduction of the cerium moment from $1.39\mu_B$ for CePt to $0.50\mu_B$ for $x=0.8$. This reduction of the magnetic moment cannot only be attributed to crystalline electric field (CEF) effects, as proved in Ref. 25, where the V_2^0 and V_2^2 CEF parameters were obtained from the susceptibility measurements on $CeNi_{0.8}Pt_{0.2}$ single crystal, yielding a magnetic moment reduction from $2.14\mu_B$ (free ion value) to $2.07\mu_B$. So, this reduction suggests that when increasing the Ni content, the Kondo interactions become more and more important, destroying the $4f$ local magnetic character.[10,25]

To clarify the peculiar magnetic properties of the $CeNi_xPt_{1-x}$ system, it would be necessary to determine how the Ce valence behaves between CePt and CeNi as well as its interplay with the competition of exchange interactions and Kondo effect driven by the modification of the hybridization between the Ce-$4f$ states and the conduction band. Trying to give a final answer to the problem we have performed a systematic XAS study at the L_1 and L_3 edges of Ce in both $CeNi_xPt_{1-x}$ and diluted $Ce_yLa_{1-y}Ni_xPt_{1-x}$ compounds.

II. EXPERIMENT

Polycrystalline $CeNi_xPt_{1-x}$ samples with compositions $x=(0,\ 0.5,\ 0.7,\ 0.8,\ 0.85,\ 0.9,\ 0.95,$ and $1)$ and $Ce_{0.35}La_{0.65}Ni_{0.8}Pt_{0.2}$ were prepared by melting pure constituents in an induction furnace under a protective argon atmosphere. X-ray diffraction and microprobe analysis have been used to check their crystallographic structure and homogeneity. All of them crystallize in the CrB orthorhombic structure ($Cmcm$ space group).

XAS measurements were made at station 7.1 of the Daresbury synchrotron. The storage ring was operated at 2 GeV with an average current of 150 mA. XAS experiments were performed in the transmission mode on homogeneous thin layers of the powdered samples at both Ce L_1 and L_3 edges. A double-crystal Si(111) monochromator was used so that a harmonic rejection of about 50% was achieved by slightly detuning the second crystal from the parallel alignment.

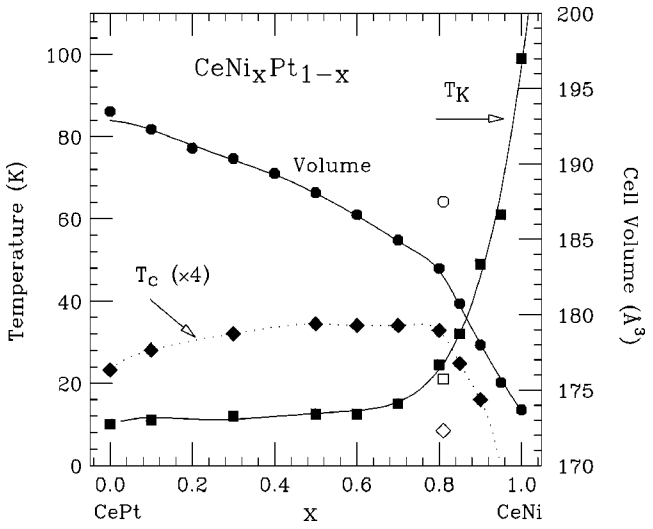

FIG. 1. Comparison between the dependence of the Curie (filled ◇) and Kondo (filled □) temperatures, and that of the cell volume (filled ○) through the $CeNi_xPt_{1-x}$ series as a function of the Ni content. The open symbols refer to the $Ce_{0.35}La_{0.65}Ni_{0.8}Pt_{0.2}$ compound.

The absorption spectra were analyzed according to standard procedures: the background contribution from previous edges was fitted with a linear function and subtracted from the experimental spectrum. Then, spectra were normalized to the absorption coefficient at ~100 eV above the edge to eliminate thickness dependence.

III. RESULTS

The Curie temperature T_c, Kondo temperature T_K and cell volume (V) of the $CeNi_xPt_{1-x}$ compounds as a function of the Ni content (x) are shown in Fig. 1.[10] We also included the data of $Ce_{0.35}La_{0.65}Ni_{0.8}Pt_{0.2}$.[18] The Curie temperatures were obtained from Arrot plots and the Kondo temperatures from the paramagnetic Curie temperatures θ_p, as extracted from susceptibility measurements. These T_K values must be considered as an estimate of the Kondo interaction strength, and they scale perfectly with those obtained from quasielastic neutron scattering[26] and from the analysis of the magnetic entropy.[17] The similarity of this Ni content dependence and the Doniach diagram is made evident in the figure. In the low-x region the RKKY interaction dominates and the system orders magnetically. For $x \geqslant 0.95$ the $4f$ conduction-band hybridization dominates and the compounds are nonmagnetic. Finally, the behavior of both T_c and T_K in the intermediate region ranging from $x=0.7$ to 0.9 suggests a comparable strength of these two interactions in such a way that the systems show Kondo-type behavior but still order magnetically. In this intermediate region T_c passes through a maximum with increasing Ni content and deviates downward until vanishing for $x>0.9$. On the other hand, the evolution of the cell volume as a function of the Ni content, also shown

in Fig. 1, presents two well-defined regions. Between CePt and $CeNi_{0.8}Pt_{0.2}$ the volume decreases linearly obeying the Vegard's law. However, for higher Ni concentrations the slope of the V versus the x curve changes abruptly indicating a faster decrease of the volume. Despite the unclear relationship between volume and valence,[27] these findings were interpreted as due to the change of cerium valence from a normal Ce^{3+} electronic state to an intermediate-valence (IV) regime.[10]

According to this interpretation $CeNi_{0.8}Pt_{0.2}$ would be close to the critical value that subdivides the phase diagram into magnetically ordered Kondo compounds and those with a nonmagnetic ground state. The emerging question is to know if the observed transition to non-magnetism corresponds to a change of valence or is simply due to the competition between the exchange interactions and the Kondo effect. However, it should be emphasized that the $4f$ conduction-band hybridization decreases with increasing cell volume, as demonstrated by the study of the La and Y substitutions.[17–19] This is the case of $Ce_{0.35}La_{0.65}Ni_{0.8}Pt_{0.2}$ shown in Fig. 1, for which the increase of the cell volume leads to the prevalence of the RKKY interaction over the Kondo effect, contrary to the case of Y-diluted series.

A. Ce L_1- and L_3-edge XAS study

Trying to clarify the influence of the Pt-Ni substitution on the electronic state of Ce in this series, we have carried out a combined study of the Ce L_3 and L_1 absorption edges in these materials. The basic idea behind the following discussion comes from the well-known relationship between the x-ray absorption coefficient, $\mu(E)$, and the angular-momentum-projected density of states, $\rho(E)$, given by

$$\mu(E) = f_{at}(E)\rho(E), \tag{1}$$

where $f_{at}(E)$ is a smoothly varying function of the probed atom that does not depend on its local environment.[28] Therefore, the absorption of x rays by excitation of lanthanide $2p$ electrons (L_3 edge) is a simple and sensitive probe of the local unoccupied lanthanide $5d$ states.[29–32] These spectra generally exhibit a pronounced peak at the absorption threshold, which corresponds to the atomiclike $2p \rightarrow 5d$ transitions, usually referred to as the ''white line.'' Changes in the shape of the white lines with increasing atomic number are driven by the localization and hybridization of the d-unoccupied states and by the progressive filling of the d band.

On the other hand, the spectral shape of the L_1-edge spectra in all the lanthanide metals exhibits a steplike rise of the absorption at the threshold, reflecting the local p-projected density of states in the band structure of the conduction electrons. However, in the solid state, a shoulderlike feature appears at the threshold, as a consequence of the overlapping of these p states with the outer s- and d-symmetry orbitals. Furthermore, when $4f$ delocalization takes place, the $4f$ electrons will also contribute at the same level to this overlapping due to the modification of the $4f$ conduction-band hybridization. Therefore, the combined study of the L_3 and L_1 absorption edges in lanthanide materials can provide a unique insight into the understanding of localization and hybridization phenomena occurring in the $CeNi_xPt_{1-x}$ series.

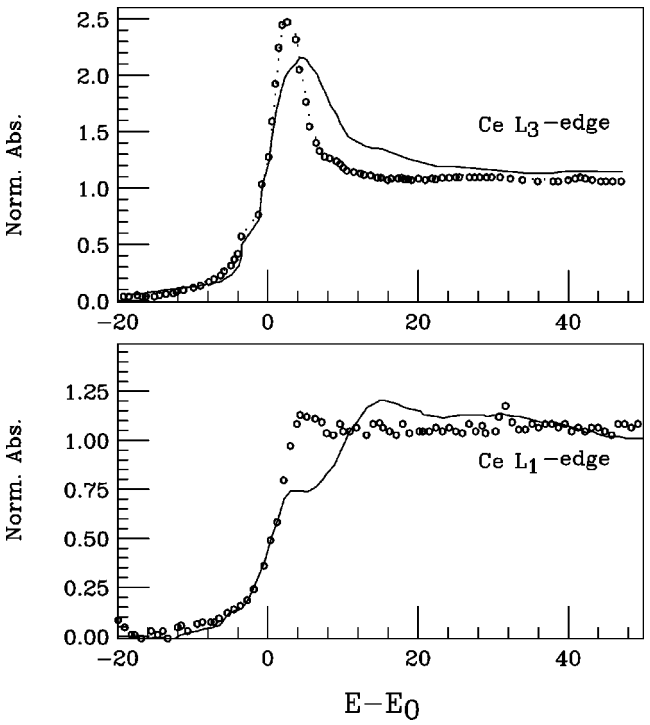

FIG. 2. L_3-edge (top panel) and L_1-edge (bottom) x-ray absorption of Ce in the vapor state (dots) at 2500 K and in the solid state (solid) at room temperature (adapted from Ref. 33).

To this end it is instructive to compare x-ray absorption of the elements in the gaseous state with the absorption in the condensed metallic state. Figure 2 shows the comparison between the $L_{1,3}$ absorption spectra of Ce in the vapor state ($\sim$2500 K) and in the solid state at room temperature.[33,34] The L_3 spectrum in the gaseous state exhibits a pronounced peak followed by a rather structureless continuous absorption. Upon condensation into the metallic state the L_3 white line does not vanish as one might naively expect from the formation of a $5d$-band with free-conduction electrons. Instead, the atomic absorption line remains largely intact: it is merely broadened and acquires a somewhat distorted, asymmetrical shape, indicating that the $5d$ states maintain a significant atomic character upon condensation. However, the overlap of the $5d$ wave functions with neighboring atoms, i.e., the hybridization or the chemical binding, causes the variation of the atomic spectral shape. Therefore, the height of the L_3 white line can be directly related to the localization of the $5d$ states according to Eq. (1).

By contrast, the L_1-edge absorption spectrum of lanthanides in the gaseous state exhibits a steplike rise of the absorption at the threshold. Upon condensation the L_1 spectra show a new double-step feature at the threshold. In the case of rare-earth vapors, such a structure is absent because the atomic resonance associated with the $2s \rightarrow 6p$ transition is very weak due to its small oscillator strength. On the contrary, the enhancement of the double-step feature in the condensed state is the experimental evidence of the strong overlapping between the outer p-symmetry orbitals with the outer

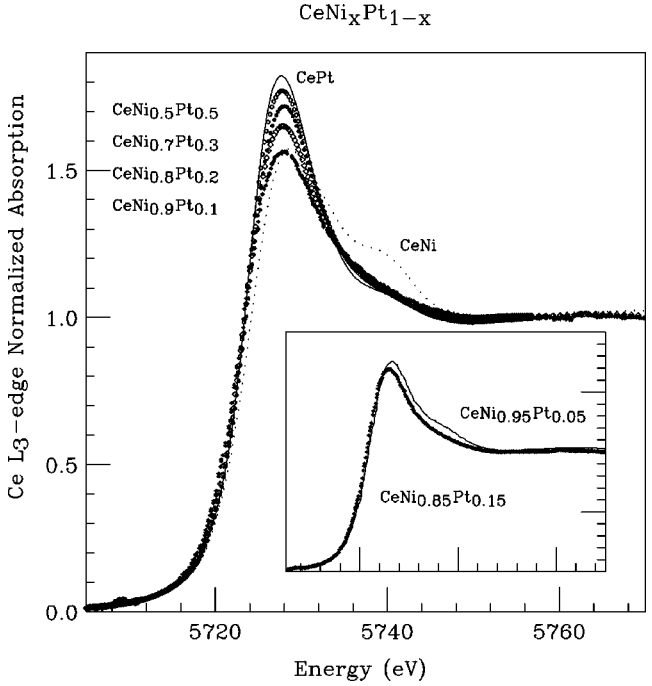

FIG. 3. Comparison of the normalized Ce L_3-edge XAS spectra through the $CeNi_xPt_{1-x}$ series for x=0 (solid line), 0.5 (○), 0.7 (solid ○), 0.8 (◇), 0.9 (solid ◇), and 1 (dotted line). The inset reports the same comparison for $CeNi_{0.85}Pt_{0.15}$, showing the normal Ce^{3+} electronic state, and $CeNi_{0.95}Pt_{0.05}$ that exhibits IV behavior.

s- and *d*-symmetry orbitals in metals, reflecting the high density of empty $5d$ states via sp-d hybridization. Therefore, the modification of the width and the intensity of the double-step near-edge structure is a fingerprint of hybridization changes of the outermost orbitals between the absorbing atom and the nearest neighbors.

Within this framework we have analyzed the Ce $L_{1,3}$-edge XAS in the $CeNi_xPt_{1-x}$ series, focusing on the evolution of the cerium electronic state from the localized Ce^{3+} character in CePt toward an IV regime in CeNi. The normalized Ce L_3-edge XAS spectra for all the investigated compounds are shown in Fig. 3. The comparison of the spectra for the two end members of the solid solution, CePt and CeNi, shows in a clear way the different electronic states of Ce in each compound. Indeed, CeNi exhibits the double-peak profile characteristic of intermediate-valence Ce-based systems, i.e., there is a mixing of the $4f^0$ and $4f^1$ configurations in the initial state. This shape reflects the superposition of the atomic $2p \rightarrow 5d$ transition for each ground-state configuration, since that of the $4f^1$ configuration shifted to lower energy as compared to the $4f^0$, due to screening effects.[35] On the contrary, in the case of CePt, only a pronounced single peak is detected at the absorption threshold, reflecting the occurrence of the Ce^{3+} electronic state in this alloy. Similar behavior is observed for the other $CeNi_xPt_{1-x}$ compounds, except for $CeNi_{0.95}Pt_{0.05}$ and CeNi. These results indicate that the localized Ce^{3+} state is preserved up to 90% of Ni substitution. What is noticeable is: (i) $CeNi_{0.8}Pt_{0.2}$, $CeNi_{0.85}Pt_{0.15}$, and $CeNi_{0.9}Pt_{0.1}$ do not exhibit intermediate valence behavior, and (ii) there is a progressive reduction of the white-line intensity with increasing Ni content in the concentration range $0 \leqslant x \leqslant 0.9$, i.e., for the compounds showing normal Ce^{3+} state. According to Eq. (1), this reduction can be interpreted as due to the delocalization of the cerium-conduction states; i.e., to the enhancement of the hybridization.

The analysis of the Ce L_3 absorption spectrum has been performed according to standard methods.[30–32] A deconvolution process was performed using a least-squares fitting procedure to fit the normalized absorption spectra to the following expression:

$$F(E) = B_0 + B_1 E + \frac{(\Gamma/2)^2 A_1}{(E-E_1)^2 + (\Gamma/2)^2} + \frac{(\Gamma/2)^2 A_2}{(E-E_2)^2 + (\Gamma/2)^2} + \frac{A_1}{A_1 + A_2}\left\{\frac{1}{2} + \frac{1}{\pi}\arctan\left[\frac{E-(E_1+\delta)}{\Gamma/2}\right]\right\} + \left\{1 - \frac{A_1}{A_1 + A_2}\right\}\left\{\frac{1}{2} + \frac{1}{\pi}\arctan\left[\frac{E-(E_2+\delta)}{\Gamma/2}\right]\right\}, \quad (2)$$

where E is the photon energy and E_1 and E_2 are, respectively, the energies of the first accessible $5d$ states in $4f^1$ and $4f^0$ configurations. Γ is the core-hole lifetime width for the considered transition and δ is the energy shift between the onset of the continuum and bound-state transitions. Finally, B_0 and B_1 are the coefficients of a linear background, while A_1 and A_2 describe the relative weights of the two configurations.[30–32]

The deconvolution procedure is illustrated in Fig. 4. In the case of the La L_3 absorption only one white line is present, which is appropriate for the existence of a unique electronic configuration for La. The absorption spectrum can be modeled by using a Lorentzian function, to simulate the atomic-like $2p \rightarrow 5d$ transition, and an arctangent function to describe the transition into the continuum states. The case of $Ce(NO_3)_4$ exemplifies the characteristic Ce L_3 absorption profile when cerium presents an intermediate valence state. In contrast to the La case there are two peaks at the edge, corresponding to the appearance of both $4f^1$ and $4f^0$ configurations. Therefore, the deconvolution of the spectrum is attained by using two pairs of Lorentzian and arctangent functions, one for each ground-state configuration. The electronic valence is estimated from the intensity ratio of the two Lorentzian functions.[30–32] As shown in Fig. 4, this procedure also describes the case of CeNi. On the contrary, the Ce L_3 absorption in $CeNi_{0.85}Pt_{0.15}$, also reported in Fig. 4, resembles the absorption profile of La, similar to compounds showing the normal Ce^{3+} electronic state. The same behavior is found for all the studied compounds with the exception of $CeNi_{0.95}Pt_{0.05}$ and CeNi (see Fig. 3), for which the deconvolution of the L_3 spectrum returns a valence of 3.13 ± 0.02 and 3.17 ± 0.02, respectively. This result is in agreement with the value 3.15 derived from x-ray emission measurements for CeNi.[36] Moreover, the Ce valence obtained for Ce in CeNi is higher than the value of 3.06 previously derived from XAS measurements by Neifeld *et al.*,[37] who, according to their classification scheme, identify CeNi as a material showing the interplay between magnetism and the Kondo

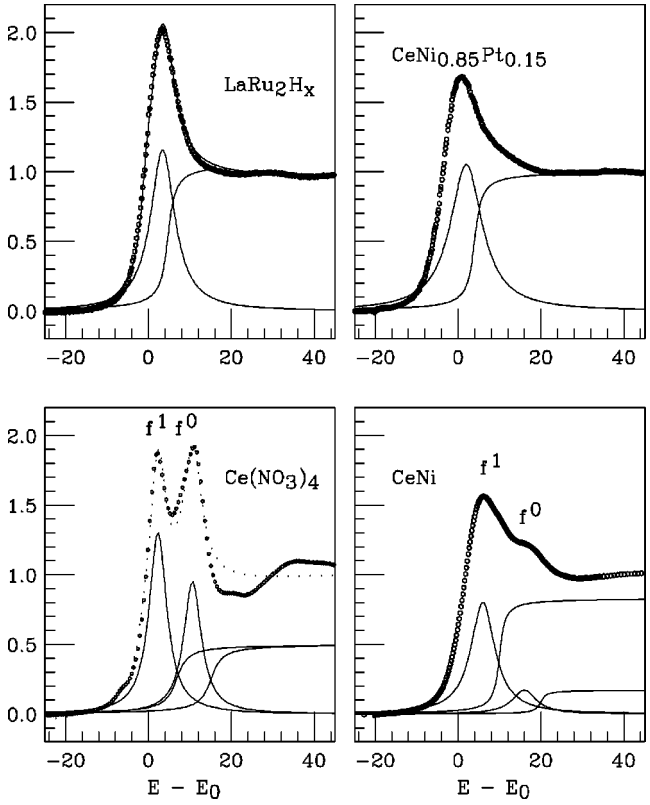

FIG. 4. Deconvolution of the normalized L_3-edge XAS spectra (see text for details).

effect. On the contrary, our estimate locates CeNi in the ''intermediate region'' of their scheme, in agreement with the nonlocalized paramagnetic behavior of this compound.

The analysis of the Ce L_3 absorption determines that the Ce^{3+} electronic state is preserved in the $CeNi_xPt_{1-x}$ series for Ni substitution $x \leqslant 0.9$ [in the following we refer to this concentration range as normal valence (NV)]. Moreover, it also supports the enhancement of the Ce *d*-state hybridization. This last result can be confirmed by the analysis of the Ce L_1-edge XAS spectra. Figure 5 shows the comparison of these spectra as a function of Ni content. As in the L_3 case, a clear difference exists between the absorption profile of the $CeNi_xPt_{1-x}$ compounds with Ni substitution below (NV) and above (IV) $x=0.9$, in agreement with the different electronic states of cerium in both regions observed at the Ce L_3 edge. Moreover, in the case of the samples belonging to the NV region, it is found that the intensity of the steplike feature at the threshold, sensitive to the *d*-state hybridization, increases as Ni content increases. Therefore, despite the indications of a Ce^{3+} electronic configuration for all the $CeNi_xPt_{1-x}$ compounds of the NV region, we observe an enhancement of the hybridization of the Ce-conduction states as Ni substitutes Pt in the system. As a consequence, although Ni substitution does not induce the transition from Ce^{3+} to an intermediate valence state in the NV region, the CePt system becomes steadily more delocalized upon Ni substitution.

B. *Ab initio* XAS calculations

To verify the interpretation that the electronic state of Ce in the $CeNi_xPt_{1-x}$ series is Ce^{3+} except for $x \geqslant 0.95$, we also

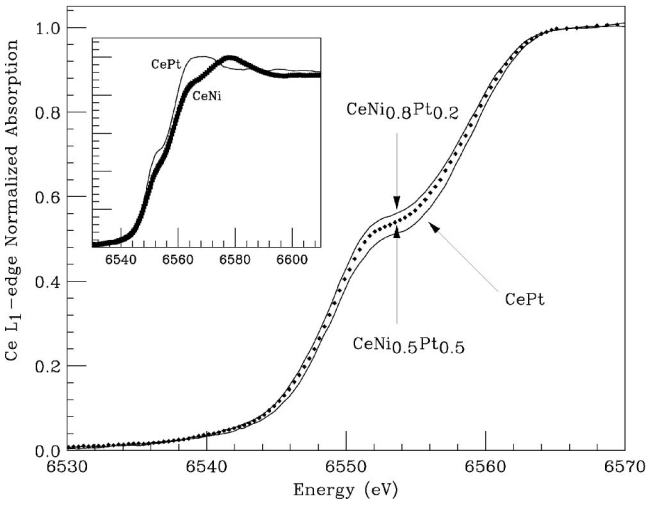

FIG. 5. Comparison of the normalized Ce L_1-edge XAS spectra in the $CeNi_xPt_{1-x}$ series.

have carried out *ab initio* computations of both Ce L_1 and L_3-edge XAS spectra. The aim of performing these calculations is to demonstrate that, despite the fact it could be argued from Fig. 1 that the IV state sets in at x=0.8, the electronic state for Ce is purely trivalent for this Ni concentration.

To this end we have computed the XAS spectra by using the multiple-scattering code CONTINUUM, based on the one-electron full-multiple-scattering theory.[38] This approximation has successfully been applied to interpret the modulations of x-ray absorption spectra in a variety of systems. However, it fails to reproduce the L_3 absorption spectrum of Ce in IV systems because of the mixing of f^0 and f^1 configurations in the ground state.[39]

The potential for the different atomic clusters was approximated by a set of spherically averaged muffin-tin potentials built by following the standard Mattheis' prescription, and by using the muffin-tin radii determined according to Norman's criterion, and by imposing a 10% overlap.[40,41] The Coulomb part of each atomic potential was generated using charge densities for neutral atoms obtained from both the tabulated atomic wave functions by Clementi and Roetti and the Herman-Skillman potentials.[42] The atomic orbitals were chosen to be neutral for the ground-state potential, whereas we follow the $Z+1$ rule to build the excited-state potential. Once the Coulomb potential has been determined from the electronic density, the construction of the scattering potential needs the addition of an exchange and correlation potential (ECP) to act as the Dyson's self-energy. We have tested different choices for the ECP part of the final-state potential: real $X\alpha$ and the energy-dependent Dirac-Hara and Hedin-Lundqvist potentials (see Refs. 43 and 44 for details). Best results have been obtained when using the complex Hedin-Lundqvist self-energy, for the exchange-correlation part of the potential whose imaginary part (related to the photoelectron mean-free path) gives the amplitude reduction due to the inelastic losses of the excited photoelectron.

Results of calculations are shown in Fig. 6 for the case of the L_1 edge, for which we have used the complex Hedin-

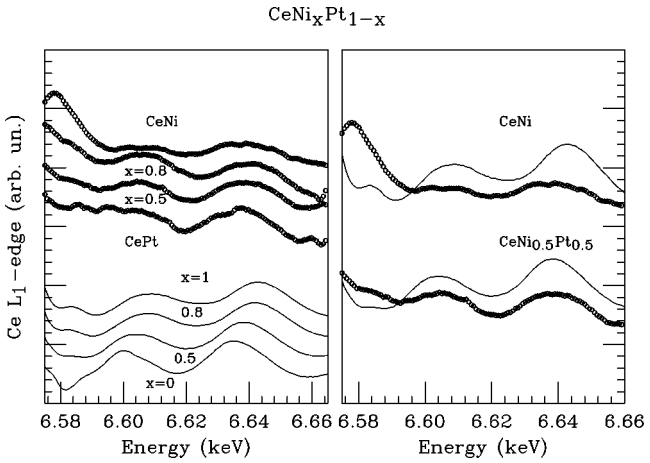

FIG. 6. Comparison between the experimental Ce L_1-edge XAS spectra of $CeNi_xPt_{1-x}$ compounds (dots) and the theoretical *ab initio* calculations (solid line) performed by imposing a Ce^{3+} electronic state for all the alloys (see text for details). CeNi and $CeNi_{0.5}Pt_{0.5}$ are displayed to stress the differences between calculated and experimental data for the former compound.

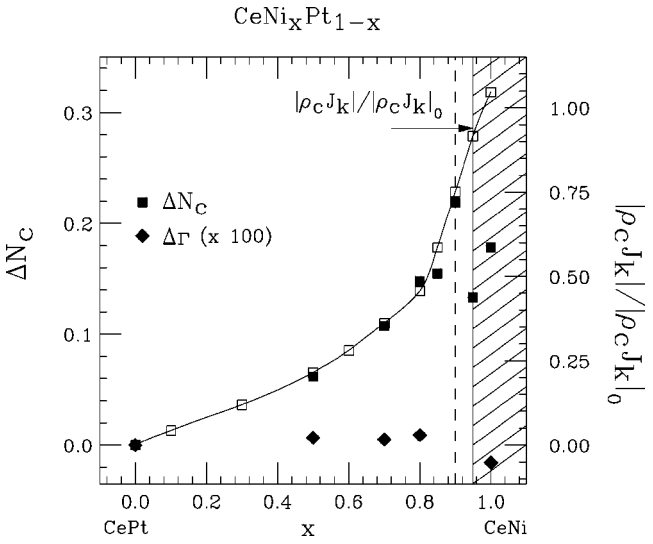

FIG. 7. Comparison of the Ni content dependence through the $CeNi_xPt_{1-x}$ series between ΔN_c (solid □) and $\Delta\Gamma$ (solid ◇) derived from the experimental XAS and $|\rho_c J_k|/|\rho_c J_k|_0$ (□) obtained according to Eq. (2). Note that the $\Delta\Gamma$ data have been multiplied by a factor 100 to be plotted in the same scale as ΔN_c. The dashed area corresponds to the range of Ni content in which the $CeNi_xPt_{1-x}$ compounds exhibit intermediate-valence behavior as determined by x-ray absorption data.

Lundqvist potential as the ECP, and Ce^{3+} as the cerium configuration in all the cases, including CeNi. Because the cell volume decreases upon Ni substitution, a shift of the XAS oscillations toward higher energy is predicted as we proceed from CePt to CeNi. This trend is confirmed by the theoretical spectra, in agreement with the experimental data for the Ce-Pt samples. However, there is a breakdown of this effect in the case of CeNi (see Fig. 6), as can be expected if this compound exhibits an intermediate-valence electronic state that cannot be explained by an electronic charge density corresponding to a Ce ion with a well-localized $4f$ electron (Ce^{3+}).

IV. DISCUSSION

The results described in the preceding sections suggest that the transition from ferromagnetism to nonmagnetism, induced in the $CeNi_xPt_{1-x}$ series as increasing the Ni content, is not due to a strong modification of the Ce valence state. On the contrary, the modification of the absorption profiles suggests a progressive enhancement of the $4f$ conduction-band hybridization, favoring the Kondo effect, as a function of Ni content. According to Eq. (1), the intensity of the L_3-XAS absorption at the edge is proportional to the local density of d states, projected on the Ce sites. The reduction of the L_3 white line upon Ni substitution is an indication of such a reduction of the density of d states. Because the valence state of Cerium is determined not to strongly change for substitutions smaller than $x=0.95$, this reduction indicates that there is a progressive delocalization of Ce d states as Ni content increases. Regarding the Ce L_1 absorption, we have shown in Fig. 2 how the shoulderlike feature at the threshold is linked to the hybridization of the outer p-, s-, and d-symmetry orbitals. In the case of rare-earth (R) metals the height of this feature reflects the density of empty $5d$ states via hybridization of the $R(sp)$ and $R(5d)$ empty states. Therefore, the increase of this intensity indicates a more delocalized nature of the $p-d$ orbitals of the rare earth, supporting the hypothesis that a higher delocalization of the $5d$ band at the Ce site takes place upon Ni substitution.

However, the conclusions based on the variation of the edge intensities [L_3 peak (P) and L_1 double-step feature (D) intensities] can appear to be only qualitative. Hence, we have normalized these variations with respect to the values exhibited by CePt. In this way, we have defined the relative variation of P and D with respect to the values found for CePt as $\Delta N_c=[P(\mathrm{CePt})-P(\mathrm{CeNi}_x\mathrm{Pt}_{1-x})]/P(\mathrm{CePt})$ and $\Delta\Gamma=[D(\mathrm{CeNi}_x\mathrm{Pt}_{1-x})\text{-}D(\mathrm{CePt})]/D(\mathrm{CePt})$. If, as discussed above, we correlate the depletion of P to the delocalization of Ce states, the defined ΔN_c corresponds to the increase of the conduction electron density, while $\Delta\Gamma$ is related to the modification of the hybridization between Ce conduction-states and those of the neighboring atoms.

The influence of the unit-cell volume (V) variation on the $|J_k\rho_c|$ product has already been derived by Lavagna, Lacroix, and Cyrot[11] and is given by

$$|\rho_c J_k| = |\rho_c J_k|_0 \exp[-q(V-V_0)/V_0], \tag{3}$$

where $|\rho_c J_k|_0$ and V_0 are the values for CePt, and q is a parameter with a value usually between 6 and 8.[45] Now, it is useful to compare the dependence on the Ni content of the $|\rho_c J_k|$ predicted for the $CeNi_xPt_{1-x}$ series with the experimentally derived parameters ΔN_c and $\Delta\Gamma$. The comparison is reported in Fig. 7. It shows good agreement between the change in the conduction-electron density obtained from the Ce L_3 data and ($|\rho_c J_k|/|\rho_c J_k|_0$) obtained according to Eq. (3). It should be noted that the soundness of the agreement holds only in the NV region. The results support our assign-

ment and the relationship between the modification of the Ce L_3-edge XAS spectrum and the conduction-electron density. Within the NV region of the $CeNi_xPt_{1-x}$ diagram, the increase of Ni content leads to the enhancement of the $4f$ conduction-band hybridization in such a way that the Kondo effect is progressively favored. This trend is contrary to that observed in the diluted $Ce_yLa_{1-y}Ni_xPt_{1-x}$ series. In the case of $Ce_{0.35}La_{0.65}Ni_{0.8}Pt_{0.2}$, ΔN_c is found to be negative. This means that Ce becomes more localized upon La substitution and that the hybridization is reduced, as would be expected because of the increase of the cell volume.

Moreover, $|\rho_c J_k|/|\rho_c J_k|_0$, ΔN_c, and $\Delta\Gamma$ show a similar trend within the NV region, while both ΔN_c and $\Delta\Gamma$ clearly depart from the $|\rho_c J_k|/|\rho_c J_k|_0$ prediction in the IV region, i.e., where Ce presents intermediate-valence behavior. These results indicate that the correlation between the $|J_k\rho_c|$ parameter in the Doniach diagram and the Ni content x in the $CeNi_xPt_{1-x}$ series holds only in the NV region. This result also indicates that for Ni concentrations between 0.8 and 0.9 the Kondo effect prevails over the RKKY interaction, so that the loss of ferromagnetic character proceeds even when the cerium electronic state is purely trivalent.

V. SUMMARY AND CONCLUSIONS

In this work we have presented an x-ray absorption spectroscopy study performed at the Ce $L_{1,3}$ edges in the intermetallic compounds $CeNi_xPt_{1-x}$ and $Ce_yLa_{1-y}Ni_xPt_{1-x}$.

The analysis of the Ce L_3-edge absorption indicates that the trivalent Ce^{3+} state is preserved in the $CeNi_xPt_{1-x}$ series up to $x \leqslant 0.9$, while Ce evolves toward an intermediate valence configuration for additional Pt substitution by Ni. This behavior has been further confirmed by the theoretical *ab initio* calculation of the XAS spectra. The modification of the Ce L_3- and L_1-edge absorption profiles has been correlated with the density of conduction electrons and with the modification of the hybridization between the $4f$ orbital of Ce and the conduction band, respectively. The validity of such an assumption has been analyzed and verified in the framework of Lavagna's model for the volume dependence of Kondo temperatures. Our results indicate that the behavior of the $CeNi_xPt_{1-x}$ series can be well accounted for by the Doniach diagram in the NV region. In other words, the identification of x as the $|J_k\rho_c|$ parameter in the Doniach diagram only holds while Ce remains trivalent. Consequently, the experimental T_K values presented for CeNi and $CeNi_{0.95}Pt_{0.05}$ in Fig. 1 should be considered as temperatures related to valence fluctuations, rather than to Kondo temperatures. Therefore, the transition to nonmagnetism observed in the $CeNi_xPt_{1-x}$ compounds is not controlled to a strong change of cerium valence, but it is the result of the competition between exchange interactions and the Kondo effect. As Ni content increases, there is a progressive enhancement of the $4f$ conduction-band hybridization that favors the Kondo effect against the long-range magnetic order of the RKKY interaction. It should be stressed that the analysis presented here could be extended to other compounds showing similar features.[46]

ACKNOWLEDGMENTS

This work was partially supported by Spanish CICYT-MAT99-0667-C01, CICYT-MAT99-0667-C04, and Aragón DGA P11/98 Grants, and by the European Science Foundation (ESF-Ferlin program).

[1] B. Coqblin, J. Ariste, A.K. Bhattacharjee, and S.M.M. Evans, in *Selected Topics in Magnetism*, edited by L.C. Gupta and M.S. Multani (World Scientific, Singapore, 1993).

[2] N. Grewe and F. Steglich, in *Handbook on the Physics and Chemistry of Rare Earths*, edited by K.A. Gschneidner, Jr. and L. Eyring (North-Holland, Amsterdam, 1991), Vol. 14, p. 343.

[3] P. Watcher, in *Handbook on the Physics and Chemistry of Rare Earths*, edited by K.A. Gschneidner, Jr. and L. Eyring (North-Holland, Amsterdam, 1994), Vol. 19, p. 177.

[4] S. Doniach, Physica B & C **91**, 231 (1977).

[5] Z. Hossain, H. Ohmoto, K. Umeo, F. Iga, T. Suzuki, T. Takabatake, N. Takamoto, and K. Kindo, Phys. Rev. B **60**, 10 383 (1999).

[6] J.R. Iglesias, C. Lacroix, and B. Coqblin, Phys. Rev. B **56**, 11 820 (1997).

[7] A.R. Ruppenthal, J.R. Iglesias, and M.A. Gusmao, Phys. Rev. B **60**, 7321 (1999).

[8] E. Pavarini and L.C. Andreani, Phys. Rev. B **59**, 8828 (1999).

[9] S. Süllow, M.C. Aronson, B.D. Rainford, and P. Haen, Phys. Rev. Lett. **82**, 2963 (1999).

[10] D. Gignoux and J.C. Gómez Sal, Phys. Rev. B **30**, 3967 (1984).

[11] M. Lavagna, C. Lacroix, and M. Cyrot, Phys. Lett. **90A**, 210 (1982); J. Phys. F: Met. Phys. **13**, 1007 (1983).

[12] D. Gignoux, F. Givord, R. Lemaire, and F. Tasset, J. Less-Common Met. **94**, 165 (1983).

[13] C. Creuzet and D. Gignoux, Phys. Rev. B **33**, 515 (1986).

[14] H. Okita, Y. Uwatoko, G. Oomi, and J. Sakurai, J. Phys. Soc. Jpn. **60**, 1856 (1991).

[15] E.S. Clementyev, P.A. Alekseev, M. Braden, J.-M. Mignot, G. Laperpot, V.N. Lazukov, and I.P. Sadikov, Phys. Rev. B **57**, R8099 (1998).

[16] S. Akari, R. Settai, Y. Inada, and Y. Onuki, Physica B **281 & 282**, 736 (2000).

[17] J.A. Blanco, M. de Podesta, J.I. Espeso, J.C. Gómez Sal, C. Lester, K.A. McEwen, N. Patrikios, and J. Rodríguez Fernández, Phys. Rev. B **49**, 15 126 (1994).

[18] D. Gignoux, J.C. Gómez Sal, J. Rodríguez Fernández, and J.M. Barandiarán, J. Phys. F: Met. Phys. **17**, L295 (1987).

[19] J.A. Blanco, D. Gignoux, J.C. Gómez Sal, J. Rodríguez Fernández, J. Voiron, and J.M. Barandiarán, J. Phys.: Condens. Matter **2**, 677 (1980).

[20] Y. Isikawa, K. Mori, A. Fujii, and K. Sato, J. Phys. Soc. Jpn. **55**, 3165 (1986).

[21] A.N. Medina, F.G. Gandra, W.R. Azanha, and L.P. Cardoso, J.

Phys.: Condens. Matter **10**, 9763 (1998).
[22] C.D. Bredl, F. Steglich, and K.D. Schotte, Z. Phys. B **29**, 327 (1978).
[23] J.I. Espeso, J.A. Blanco, M. Reiffers, J. Rodríguez-Fernández, and J.C. Gómez Sal, J. Magn. Magn. Mater. **157&158**, 685 (1996); J.I. Espeso, Ph.D. thesis, Universidad de Cantabria, Santander, Spain, 1995.
[24] J.C. Gómez Sal, J.I. Espeso, J. Rodríguez-Fernández, J.A. Blanco, and J. Rodríguez Carvajal, Solid State Commun. **87**, 863 (1993).
[25] G. Fillion, M.A. Fremy, D. Gignoux, J.C. Gómez Sal, and B. Gorges, J. Magn. Magn. Mater. **63&64**, 117 (1987).
[26] J.A. Blanco, J.C. Gómez Sal, J. Rodríguez-Fernández, J. Sandonís, and J.M. Barandiarán, Physica B **100-101**, 217 (1992); J.A. Blanco, J. Sandonís, J. Rodríguez-Fernández, J.C. Gómez Sal, F. Plazaola, and J.M. Barandiarán, in *Quasielastic Neutron Scattering*, edited by J. Colmenero, A. Alegría, and F.J. Bermejo (World Scientific, Singapore, 1994), p. 211.
[27] D. Wöhlleben and J. Röhler, J. Appl. Phys. **55**, 1904 (1984).
[28] J.E. Müller and J.W. Wilkins, Phys. Rev. B **29**, 4331 (1994).
[29] A. Bianconi, in *X-ray Absorption: Principles, Applications, Techniques of EXAFS, SEXAFS and XANES*, edited by D.C. Koningsberger and R. Prins (Wiley, New York, 1988), Chap. 11, and references therein.
[30] See, for example, J. Röhler, in *Handbook on the Physics and Chemistry of Rare Earths*, edited by K.A. Gschneidner, Jr., L. Eyring, and S. Hufner (North-Holland, Amsterdam, 1987), Vol. 10.
[31] J. Chaboy, A. Marcelli, and L. Bozukov, J. Phys.: Condens. Matter **7**, 8197 (1995).
[32] J. Chaboy, J. García, and A. Marcelli, J. Magn. Magn. Mater. **166**, 149 (1997).
[33] G. Materlik, B. Sonntag, and M. Tausch, Phys. Rev. Lett. **51**, 1300 (1983).
[34] G. Materlik, J.E. Müller, and J.W. Wilkins, Phys. Rev. Lett. **50**, 267 (1983).
[35] S.M. Blokhin and E. Ye. Vaynshteyn, Fiz. Met. Metalloved. **19**, 371 (1965).
[36] A.E. Sovestenov, V.A. Shaburov, and K.I. Kozlow, Fiz. Tverd. Tela (Leningrad) **23**, 2827 (1981) [Sov. Phys. Solid State **23**, 1652 (1981)].
[37] R.A. Neifeld, M. Croft, T. Mihalisin, M. Madigan, M.S. Torikachvili, M.B. Maple, and L.E. DeLong, Phys. Rev. B **32**, 6928 (1985).
[38] See, for example, C.R. Natoli and M. Benfatto, J. Phys. (Paris), Colloq. **47**, C8-11 (1986), and references therein.
[39] J.A. Solera, J. Garcia, and M.G. Proietti, Phys. Rev. B **51**, 2678 (1995).
[40] L.F. Mattheis, Phys. Rev. **133**, A1399 (1964); **134**, A970 (1964).
[41] J.G. Norman, Mol. Phys. **81**, 1191 (1974).
[42] E. Clementi and C. Roetti, At. Data Nucl. Data Tables **14**, 177 (1974); F. Herman and S. Skillman, *Atomic Structure Calculations* (Prentice-Hall, Englewood Cliffs, NJ, 1963).
[43] J. Chaboy and S. Quartieri, Phys. Rev. B **52**, 6349 (1995).
[44] T.A. Tyson, K.O. Hodgson, C.R. Natoli, and M. Benfatto, Phys. Rev. B **46**, 5997 (1994).
[45] A.N. Medina, M.A. Hayashi, L.P. Cardoso, S. Gama, and F. G. Gandra, Phys. Rev. B **57**, 5900 (1998).
[46] J.G. Sereni, Physica B **281 & 282**, 337 (2000).